Copyright © 2005 American Scientific Publishers
All rights reserved
Printed in the United States of America

Journal of
Biomedical Nanotechnology
Vol. 1, 1–8, 2005

Fabrication of Microfluidically-Accessible Planar Nanoholes on Elastomeric Substrates

Nicholas L. Stucky, Chihchen Chen, T. Fettah Kosar, and Albert Folch*

Department of Bioengineering, University of Washington, Campus Box 352255, Seattle, WA 98195, USA

Here we present two novel fabrication techniques for creating planar nanohole devices designed for making measurements or delivering soluble compounds to a number of single cells simultaneously. The devices are micromolded in poly(dimethylsiloxane) (PDMS). In both designs presented here, the nanoholes are arranged in a linear array on a flat surface; each nanohole constitutes a fluidic connection or nanochannel between two volumes, the one above the surface and a microfluidic channel beneath the surface dedicated to that nanohole. Cells can be immobilized and cultured on the planar array surface either directly on top of the nanoholes or in close proximity. The integration of nanochannels at the terminal end of an underlying microchannel network provides nanometer-scale precision and favorable optical properties while allowing for low fluidic and electrical resistance.

Keywords: Nanohole, Nanoaperture, Electron Beam Lithography, Soft Lithography, BioMEMS, Microfluidics.

RESEARCH ARTICLE

1. INTRODUCTION

Biologists and biophysicists increasingly use micro- or nano-scale tools for cell studies. An example of a nanoscale-probing tool is the commonly utilized glass micropipette. Such micropipettes are essentially thin-walled glass capillary tubes that are heated and extruded to produce a "tip" end; the tip is shaped like a hollow cone ending in a small hole or aperture. The heat and force applied during the pulling process can be adjusted to provide the desired diameter of the tip aperture, ranging from submicron to tens of microns. Micropipettes are inexpensive, ubiquitous in biological laboratories, and their protocols have been established for decades. Common applications of micropipette techniques include microinjection for intracellular delivery,[1] cell immobilization through aspiration for cell deformation studies,[2] "puffing" (pressure ejection) for chemotactic and cellular guidance studies,[3,4] and electrophysiological recordings.[5,6] Unfortunately, micropipette techniques also have several key constraints. Expensive micromanipulators and cumbersome vibration isolation schemes are required to precisely position micropipette tips inside, outside, or in contact with the cell membrane. Even with these precautions, vibrational disturbances are still a common cause of experimental failure, resulting in low yields in applications such as patch-clamp electrophysiology. In addition, existing micropipette techniques require considerable operator input and proceed at a slow, serial pace. Last but not least, the bulky setup and peripheral equipment required by micropipettes make it difficult, if not impossible, to probe many cells simultaneously. Due to these limitations, recently several alternatives to produce micro- and nanoscale apertures for cell studies have been proposed.

All these alternative methods are based on a similar concept often termed the "planar aperture." The cells are brought into contact with a micron or submicron aperture on a planar surface (henceforth referred to as a "nanohole," e.g., a 1 μm-diam. hole fabricated using nanopatterning techniques is also termed a nanohole). Methods differ in the fabrication process and materials used to fabricate the nanoholes. Substrates made of silicon, glass, silicon nitride, and the elastomer poly(dimethylsiloxane) (PDMS) have been used. Well-defined nanoholes have been constructed using micro- and nano-fabrication techniques such as ion track etching,[7,8] ion-beam sculpting,[9] electron-beam lithography (EBL),[10] or conventional silicon-based patterning/etching techniques.[11,13] These devices, by virtue of being compact, generally feature very low vibration sensitivity compared to micropipettes. In addition, the use of microfabrication techniques enables integration of fluid addressing systems, control of aperture size, and tailoring of the number of apertures per device. Planar nanohole devices have been demonstrated for applications such as immunoisolation,[11] biomolecular separation,[11] chip-based patch-clamping,[7,12,14,17] lipid bilayer-based single ion channel studies,[13] and single-molecule DNA sequencing.[9] However, existing planar nanohole fabrication methods

*Authors to whom correspondence should be addressed.

suffer from certain shortcomings. Some techniques (e.g. ion track etching and ion beam sculpting) require equipment that is prohibitively expensive and/or inaccessible to most researchers. In the majority of these devices, microfluidically addressing nanoholes has yet to be accomplished.

An attractive strategy is the replica-molding of nanoholes in the biocompatible elastomer PDMS, which can be micromolded inexpensively using soft-lithography.[18] PDMS has many favorable properties. PDMS is optically transparent down to 300 nm and biocompatible. PDMS can be cured at low temperature, can replicate features with submicron fidelity, and can be surface-modified using a short treatment with oxygen plasma; the surface oxidation allows for covalently binding PDMS to PDMS or clean glass.[19,20] One PDMS nanohole fabrication method creates planar nanoholes by curing PDMS over a small aperture in a metal plate while air is ejected.[21] Unfortunately, the well-defined planar nanoholes are not microfluidically addressed nor can be produced in a dense array configuration. A different PDMS-based design uses standard lithography and PDMS micromolding to create well-defined microfluidically-addressed nanoholes in a dense configuration;[14] however, the nanoholes created by this method do not emerge from a planar surface; rather, due to design constraints, the nanoholes must emerge from the corner of a wall, which limits applications of the device. For example, while successful whole-cell patch clamp recordings were demonstrated, the yield of high-quality cell seals (>1 GΩ) is lower than reported in previously described planar devices.[21] Though the cause of the low yield was unclear, it is plausible that the low yield is exacerbated by the non-planar architecture.

To further improve on these advancements, we have developed two methods to fabricate microfluidic devices that incorporate microfluidically-addressable nanoholes in planar topographies. Device design I, which we term the "sliced design," uses slicing with a microtome to create the planar surface. Device design II, which we call the "inflated design," employs a PDMS micromolding technique based on inflatable molds[22] to create planar nanoholes. In both device designs, each nanohole is connected to ("addressed by") a different microchannel connected to that nanohole. We expect that both designs will permit multiple simultaneous single-cell stimulation and measurement.

2. MATERIALS AND METHODS

2.1. SU-8 Master Fabrication

A 3-inch diameter, 400 μm-thick Si⟨100⟩ wafer (Silicon Sense, Inc., NH) was used as the substrate for the first lithography step in the fabrication process. In this step electron beam lithography (EBL) was utilized as a method for directly patterning SU-8 negative photoresist (MicroChem Corp., MA) on the wafer substrate (Fig. 1a). SU-8-2 resist was spun on the wafer at 1000 rpm for 30 seconds to create a 2 μm-thick layer. A set of 200 μm-long, 2 μm-wide

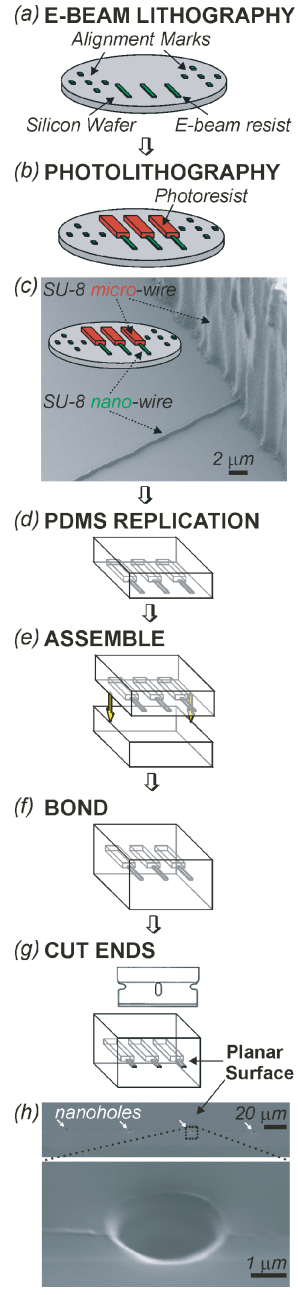

Fig. 1. Fabrication of planar nanoholes by slicing ("sliced design"). (a) First, an array of straight "nanoscale" lines (2 μm × 2 μm cross section, shown in green) was created by electron-beam lithography. (b) A set of microscale lines (30 μm × 40 μm cross section, shown in red) was photolithographically patterned in alignment with the existing nanoscale lines. (c) An SEM image of the master showing both nano- and microscale SU-8 features. (d) The master is replicated in PDMS. (e) The PDMS replica is capped with a slab of PDMS and (f) chemically bonded together, forming dead-ended PDMS nanochannels (each nanochannel addressed by one microchannel). (g) The PDMS device was cut by a microtome blade to reveal nanoholes on a flat surface. (h) SEM images of an array of four nanoholes (top) and a close-up of one of the nanoholes (bottom).

lines and alignment marks for the subsequent photolithography step were patterned. EBL was performed in a field-emission scanning electron microscope (SEM) (Sirion; FEI Company, OR) interfaced with a pattern generation system (Nabity Lithography Systems, MT) that accepts standard computer-aid design (CAD) files. The alignment marks were covered with adhesive tape and the wafer was coated using a spin coater (Solitec Model 4110, Solitec Wafer Processing, Inc., CA) set at 4000 rpm for 30 seconds to create a 40 μm-thick layer of SU-8-50 photoresist. In the second lithography step, the alignment marks are used to register the existing nanoscale features with the features in the second layer (printed in a high-resolution acetate film photomask; Publication Services, University of Washington). Next, standard photolithography is employed to expose and develop the wafer. The result is an SU-8 master wafer with microscale circuit, with each "wire" connected to inlet and outlet pads at their ends and to nanoscale lines at their center (Fig. 1b). Figure 1c shows an SEM image of the master at a location where a SU-8 "micro-wire" connects to a SU-8 "nano-wire."

2.2. Fabrication of a Planar Array of Nanoholes in PDMS by Slicing ("Sliced Design")

The sliced design was created by replicating the master in PDMS (Sylgard 184; Dow Corning, MI) using standard soft-lithography methods. Briefly, the master was silanized by exposure to a vapor of (tridecafluoro-1,1,2,2-tetrahydroocytyl)-1-trichlorosilane (United Chemical Technologies, Bristol, PA) in house vacuum at room temperature for 30 min. The PDMS precursor (10:1 weight ratio of elastomer to curing agent) was poured over the silanized master, degassed in a desiccator, and allowed to cure overnight in an oven at 65 °C (Fig. 1d). The PDMS replica of the master was bonded after activation by 30 seconds of oxygen plasma treatment (300 W, 1 torr) to a similarly treated 5 mm-thick planar PDMS backing sheet (Fig. 1e). (This backing sheet was created by curing PDMS over a silanized silicon wafer.) The SU-8 master can be replicated multiple times in PDMS. In order to make a multilayer device the PDMS replica layers must be stacked. The bonding surfaces of adjacent layers were both treated with oxygen plasma, aligned visually under a stereomicroscope and brought together to form an irreversible seal (Fig. 1f). This process can be repeated an arbitrary number of times to create a two-dimensional array of nanochannels connected to microchannels. The nanochannels are replicas of the nanoscale line features of the SU-8 master. In the last fabrication step, a tissue-culture microtome (Tissue Slicer 2/Digital Micrometer, The Vibratome Company, St. Louis, MO) was used to slice perpendicularly through the nanochannels near the terminal end of the microchannel. This process created a planar surface containing an array of nanoholes, with each nanohole connected to a dedicated microchannel (Fig. 1g).

2.3. Fabrication of a Planar Array of Nanoholes in PDMS Using Inflatable Micromolds ("Inflated Design")

The inflated design utilized inflatable molds.[22] The inflatable molds consist of microscale cavities under a flat surface; as the cavities are pressurized, the surface acquires a microtopography at the positions right above the cavities. The cavities are built by capping a set of PDMS microchannels with a thin PDMS membrane. The deflections of the membrane can be controlled by tuning the applied pressure and can be replica-molded in PDMS. The masters for the inflated-design devices were made with the same two-step process (EBL followed by photolithography) as in the sliced design (Figs. 2a–c). To fabricate the PDMS membrane, PDMS precursor (10:1 weight ratio of elastomer to curing agent) was diluted with hexane at a 3:1 weight ratio and spun on top of a silanized silicon wafer at 7000 rpm. The wafer was then placed on a hot plate at 85 °C for 4 minutes to allow the PDMS to cure. This process created a PDMS membrane approximately 11 μm thick. The membrane was then irreversibly bonded to the PDMS replica (Figs. 2d–e). Positive pressure of varying magnitude (from 4 to 34 kPa) was applied to the closed channels to deflect the membrane (Fig. 2f). The deflected membrane was then recast in PDMS to set the new curved roof of the channel (Fig. 2f). The device could be used with the microfluidic reservoir intact or sliced (Fig. 2g); slicing this device creates direct access to the volume above the planar surface (e.g., cells can be directly deposited on the surface without further fluid addressing).

2.4. Electrical Characterization and Comparison of the Nanohole Devices

A convenient method for measuring the integrity of the nanoholes and nanochannels is to measure the electrical resistance of the fluidic path through the device. For these experiments the microchannels were filled with an "extracellular solution" consisting of NaCl 120 mM, KCl 20 mM, $CaCl_2$ 2 mM, $MgCl_2$ 2 mM, D-glucose 10 mM, and HEPES (4-(2-hydroxyethyl)piperazine-1-ethanesulfonic acid) 10 mM.[23] The pH was adjusted to 7.4 with NaOH. The electrical resistance of the device could be measured by applying a square wave voltage between the two Ag/AgCl electrodes placed on opposite sides of the nanochannel. The electrodes were created by dipping a 0.25 mm-diam. silver wire (World Precision Instruments Inc., Sarasota, FL) in molten AgCl (Sigma-Aldrich Co., St. Louis, MO). Experiments were conducted using a conventional setup for patch clamp recording. Briefly, a patch clamp amplifier (Multiclamp 700A; Axon Instruments Inc., CA) was used to apply a square wave

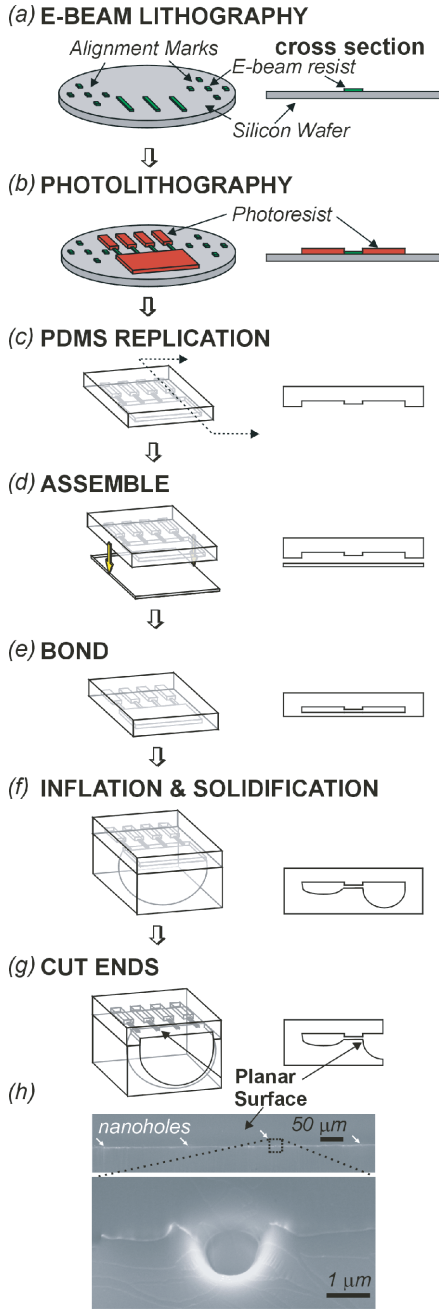

Fig. 2. Fabrication of planar nanoholes using an inflatable mold ("inflated design"). (a) First, an array of 1 μm × 1 μm cross sectional lines (shown in green) was created by electron-beam lithography. (b) Second, microscale features (shown in red) were photolithographically patterned in alignment with the existing nanoscale lines. (c) PDMS replica made by casting and curing PDMS against the master. (d) The PDMS replica was capped with a thin (11 μm-thick) spin-coated PDMS membrane and (e) chemically bonded together. (f) The PDMS device was put in vacuum, which expanded the air trapped in the reservoir (capped with the PDMS membrane) very much like a balloon; this procedure created a flat surface at the openings of nanochannels. A small amount of PDMS was poured on top of the PDMS balloon and cured, which solidified the balloon walls. (g) If desired, the PDMS device can be cut open to facilitate access to the planar surface. (h) SEM images of an array of four nanoholes (top) and a close-up of one of the nanoholes (bottom).

voltage step (~5 mV amplitude) across the electrodes. The electrical current through the device was digitized by a data acquisition system (Digidata 1322, Axon Instruments Inc., CA) and recorded in a computer by commercially-available software (pCLAMP 8.0; Axon Instruments Inc., CA). The electrical resistance of the fluidic path through the device was calculated using Ohm's Law, i.e., dividing the applied voltage step by the steady-state current.

2.5. Biocompatibility of the Nanohole Device

Rat basophilic leukemia (RBL-1) cells were used as a model system for immobilization studies. These cells were chosen because they can be cultured in suspension and are commonly used in electrophysiology for studying endogenous ion channels. Cells were obtained from American Type Cell Culture (Manassas, VA) and maintained according to the previously published protocol.[24] Murine skeletal muscle (C2C12) cells were also used for biocompatibility assessments and were obtained from American Type Cell Culture (Manassas, VA) as well. C2C12 cells were cultured as described by Tourovskaia et al.[25] C2C12 myoblasts were seeded above the nanoholes on the planar PDMS surface of the sliced design devices. No surface treatment was performed on the cell-seeding surface. Phase-contrast images were taken after 14 hours using an inverted microscope.

2.6. Cell Immobilization

RBL-1 cell suspensions were centrifuged at 120 g for 5 minutes. After each centrifugation step, the supernatant was removed and the cells were re-suspended in fresh extracellular solution. This process was repeated twice to remove cellular debris. After the final re-suspension, the cells were introduced into the "cell reservoir." We term "cell reservoir" the large volume into which the cells are typically introduced; in contrast, the microchannels (connected to the end of the nanochannel opposite to the cell reservoir) are designed to deliver chemical or electrical stimulation. In the sliced design, the cell reservoir was created opposite the microchannels by cutting open the device. In the inflated design, a large (6 mm × 6 mm) cell reservoir is replicated from a similarly sized feature on the SU-8 master.

Pressure differentials across the nanochannel were used to hydrodynamically move fluid and cells to the nanohole outlets. For both sliced and inflated-design devices, negative pressure differentials were created by connecting a vacuum line via a pressure regulator (Conoflow Brass Regulator 0-5 psi, Technical Controls, Portland OR) to the microchannels and maintaining the other side of the nanochannel (cell reservoir) at atmospheric pressure. In the inflated-design devices (featuring closed cell reservoirs), positive pressure differentials were applied by connecting a nitrogen gas cylinder to the cell reservoir via a pressure

regulator. The microchannel side of the nanochannel was maintained at atmospheric pressure.

3. RESULTS AND DISCUSSION

3.1. Fabrication of a Planar Array of Nanoholes in PDMS by Slicing ("Sliced Design")

The sliced design produced arrays of nanoholes with consistent dimensions (Fig. 1h) but unexpected geometry: the nanoholes were elliptical with dimensions of 2.5 μm along one axis and 1.5 μm along the other axis, whereas the nanoscale lines in the master (see Fig. 1c) had an approximately square cross section. Corner rounding may occur after molding and following bonding due to the exposure of the PDMS surfaces to an oxygen plasma (which is known to introduce surface mechanical stress;[26]) alternatively, rounding may be present only on devices that were coated with a thin (~12 nm) film of gold (also known to introduce surface stress[27]) as sample preparation for SEM imaging. We also noticed that the interface between two bonded PDMS layers is visible in SEM images (see Fig. 1h and Fig. 2h), which supports the notion that the mechanical stress is present at the PDMS–PDMS interface and not at the gold-coated surface (hence the rounding is real). In any case, we have not further investigated the reason for this distortion nor tried to prevent it because round nanohole rims, if real, are in principle more suitable for immobilizing cells (which are spherical) than rims with square corners.

The first proof-of-concept device featured a single row of 4 planar nanoholes. The incorporation of inlet and outlet microchannels allowed each nanohole to be individually addressed and permitted straightforward and rapid fluid exchange. Two-dimensional arrays incorporating more nanoholes were easily created by stacking and bonding several PDMS replicas. Unfortunately, opening the channels by slicing with the microtome yielded high device-to-device variability in the length of the nanochannels (see below for a detailed discussion on variability in the comparison between the two designs). Using a stereomicroscope, a slice through the nanochannels could be made on average within 200 μm of the ends of the microchannels; the precision of the slice location was limited to $+/-100$ μm. This created an approximately 200 μm device-to-device variability in the lengths of the nanochannels. In addition, the slicing technique created a microscopically rough cell-seeding surface, resulting in phase-contrast microscopy images that were somewhat blurry (Fig. 4a).

3.2. Fabrication of a Planar Array of Nanoholes in PDMS Using Inflatable Micromolds ("Inflated Design")

Similarly to the sliced-design devices, the inflated-design devices featured planar surfaces with nanoholes that consistently had rounded (~1 μm-diameter) cross sections. These devices also featured 4 nanoholes. The inflated-design devices avoided the poorly controlled channel lengths typical of the sliced-design devices. In the inflated design, the lengths of the nanochannels were determined by the high precision of the photomask features and our alignment resolution. In the sliced design, in contrast, the nanochannel lengths were affected by poor control over the placement of the blade relative to the device and over the orientation of the blade's slicing plane during the slicing step. The cell-seeding surface created by replication of the vertical SU-8 walls in the inflated design was smoother than the surface created by slicing, as assessed by SEM imaging (data not shown).

3.3. Comparison of Electrical Characteristics of the Nanohole Devices

To measure the resistance of the nanochannels R_{nCh}, the resistance of the microchannels $R_{\mu Ch}$ was subtracted from the overall resistance based on the known microchannel dimensions (length L and cross-sectional area A) and the resistivity ρ of the solution ($= 0.512 \Omega \cdot m$), $R_{\mu Ch} = \rho\ L/A$. The nanochannel resistance R_{nCh} in the sliced design (number of nanochannels analyzed $n = 16$) had a maximum variability from device-to-device of $\Delta R_{nCh} =$ 66.4 MΩ (absolute range: 1.4 MΩ to 67.8 MΩ, standard deviation 17.3 MΩ). On the other hand, the nanochannel resistance in the inflated design ($n = 11$) varied within only $\Delta R_{nCh} = 12.3$ MΩ (absolute range: 4.4 MΩ to 16.7 MΩ, standard deviation 6.8 MΩ). The graph in Figure 3 clearly illustrates the consequences of highly variable nanochannel length on the electrical properties of the device. A plot of the sequence of all the measurements for both designs shows the differences in device-to-device resistance variability as well as variability in electrical resistance between

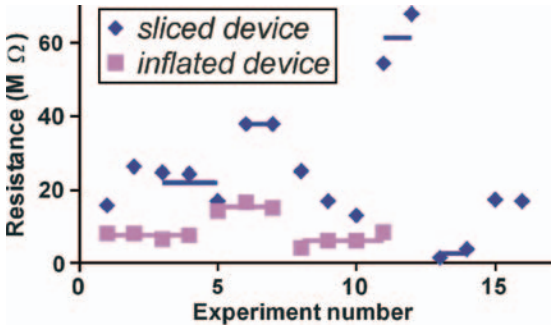

Fig. 3. Characterization of the electrical resistances of various devices. Symbols indicate resistance of sliced-design devices (Design I) (♦) and inflated-design devices (Design II) (■). The electrical resistance was measured with a pair of Ag/AgCl electrodes placed across the nanochannel and microchannel network filled with electrolyte (resistivity = 0.512 $\Omega \cdot$ m). The fraction of the total resistance attributable to the microchannel has been subtracted (see text). The mean resistance values corresponding to nanochannels in the same device are shown as short horizontal lines.

RESEARCH ARTICLE

nanochannels on the same device (mean values of resistance corresponding to the nanoholes in a given device are represented in Figure 3 as horizontal lines). It should be noted that the nanochannel resistance contributes significantly to the total resistance of the devices. For a typical sliced-design device, the nanochannel was approximately 200 μm long and was responsible for 55% of the total electrical resistance of the device. On the other hand, nanochannels in the inflated-design devices could consistently be produced with lengths less than 20 μm. The nanochannel shape could also be designed with a triangular taper to increase the cross-sectional area and thereby further lower the resistance beyond that of a linear nanochannel (see Fig. 4b).

A large variability in *electrical* resistances can be detrimental to electrophysiological experiments where it is essential to separate the electrical contributions of the cell from those that can be attributed to the device and supporting electronics. In addition, variations in the device-to-device *fluidic* resistances can complicate experiments where flow or pressure drops need to be consistent, such as during cell immobilization or fluid ejection. Last but not least, variations in nanochannel length can become a hurdle in experiments where the diffusion of molecules along the nanochannel is critical.

3.4. Biocompatibility of the Nanohole Device

Images of C2C12 myoblasts seeded above the nanoholes on the planar PDMS surface of the sliced design devices taken at 14 hours after cell seeding showed healthy and normal cell morphology. Phase-contrast images showed slight phase distortions in the regions directly above the microchannels (Fig. 4a). Phase-contrast distortion was not an issue for the inflated-design devices because their design allowed more convenient side imaging of the nanochannel and cells (Fig. 4b).

3.5. Cell Immobilization

By applying pressure differentials between 1 and 3 psi, flow (of the cell suspension) was established from the cell reservoir to the microchannels through the nanochannels, effectively bringing the cells to the nanoholes. The cells were observed to immobilize immediately atop the nanoholes, obstructing them (Fig. 4b). Further evidence of fluidic obstruction included an increase in electrical resistance simultaneously with cell immobilization. In cases of extreme pressure differentials (3–5 psi) cells were forced through the nanochannel (Fig. 4c). Interestingly, different cellular constituents passed through the nanochannel at different rates, resulting in separation: nuclear material (labeled blue with 4′,6-diamidino-2-phenylindole (DAPI) (Molecular Probes, Carlsbad, CA)) passed through the nanochannel faster than the cytoskeleton (labeled green with Alexa 488-labeled phalloidin (Molecular Probes, Carlsbad, CA)). Given constraints imposed by the design, the cell immobilization procedure differed for different designs. The sliced design did not allow for pressure lines being attached to the cell reservoir, so applied pressure

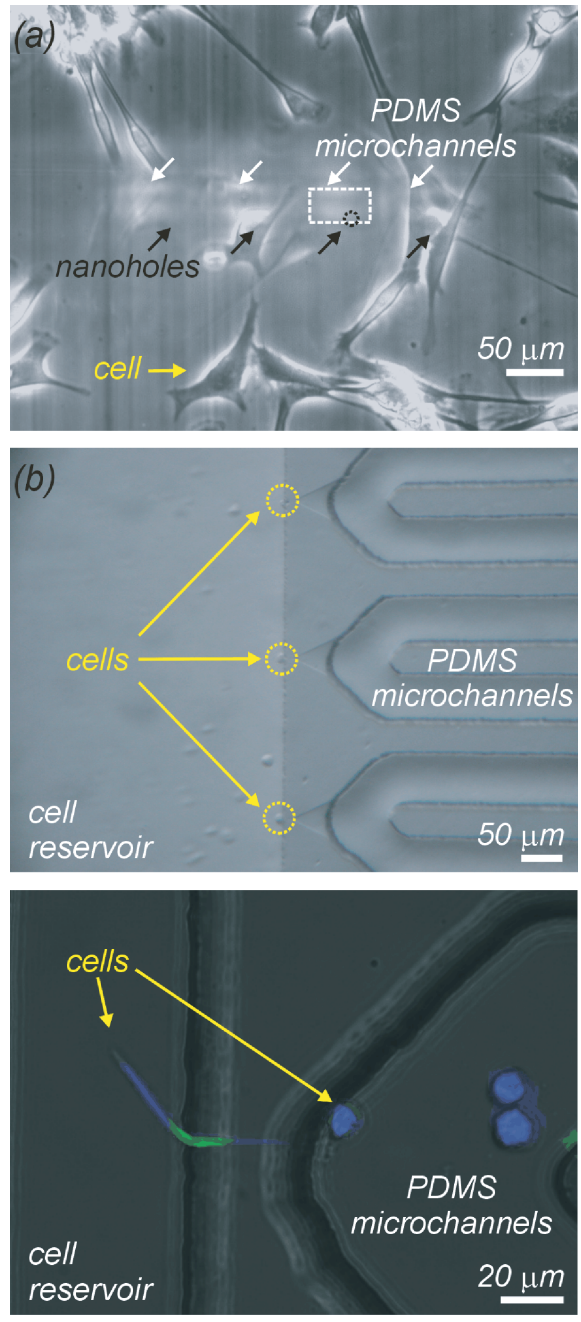

Fig. 4. Cell immobilization on planar nanohole devices. (a) Phase-contrast image of C2C12 myoblasts seeded on a sliced-design planar PDMS nanohole device imaged 14 hours after cell seeding. No surface treatment was performed on the cell-seeding surface. Note that phase-contrast is distorted in the regions directly over the microchannels. (b) Single RBL-1 cells immobilized on the planar nanoholes of an inflated-design device. (c) Overlay of phase-contrast and fluorescence images of RBL-1 cells fixed with paraformaldehyde after a cell has been forced through the nanohole. Fluorescence shows phalloidin staining of the cytoskeleton (in green) and DAPI staining of the cell nucleus (in blue).

differentials had to be applied via the microchannels. In order to drag cells to the nanohole, vacuum (∼1–3 psi value) was connected to the microchannels while the cell reservoir was at atmospheric pressure. Unfortunately, because PDMS is a gas-permeable polymer, microchannel pressures in the range 1–3 psi below atmospheric pressure were sufficient to occasionally induce bubble formation inside the microchannels. Therefore, for applications where bubble formation is not tolerable, the range of pressures that can be used with the sliced-design device is limited to low (<1 psi) pressures.

In experiments conducted using inflated-design devices, cell immobilization was achieved by applying a positive pressure to the cell reservoir and maintaining the microchannels at atmospheric pressure, thus causing hydrodynamic flow from the cell reservoir into the microchannels. Typically, a pressure differential of 1.5 psi was sufficient to drive cells to nanoholes in the inflated design. Occasionally, higher pressures up to 3 psi were used when the microchannel was partially blocked or not entirely filled with fluid (pressurization causes the trapped air to diffuse into the PDMS walls). Once the cells are immobilized, the nanohole is effectively a nanoscale probe to record from or stimulate a cell on a sub-cellular scale. We are currently investigating electrophysiological applications and local uptake of enzymatic substrates using these devices.

4. CONCLUSIONS

Planar nanoholes obviate traditional setups for cell immobilization such as micromanipulators and vibration isolation tables and can potentially be used to deliver biochemical factors or electrical stimuli to arrays of single cells and to record the electrophysiological activity of multiple cells simultaneously. We have demonstrated the immobilization of single cells on nanoholes molded on a PDMS planar surface. PDMS is a convenient material for fabricating nanoholes because it provides for inexpensive replica-molding, optical transparency down to 300 nm, chemical inertness, biocompatibility, and electrical insulation. The fabrication time, from lithography to completed device, can take less than a day, so it is well suited for rapid prototyping and for tailoring to specific applications. We have tested two designs, both incorporating linear nanohole arrays with an integrated underlying microfluidic network. Stacking of the devices allows for two-dimensional arrays of nanoholes. Inflated-design devices have well-defined nanochannel lengths and little device-to-device variability. The microfluidic network in conjunction with more sophisticated pressurization switches can potentially be used to automate the perfusion of cells with various compounds, e.g., for applications such as biotechnology (e.g. pharmacology and drug discovery) and cell biology (e.g. electrophysiology and neuroscience).

Acknowledgments: We are grateful to Anna Tourovskaia for providing assistance with C2C12 cells. Microfabrication was conducted at the Washington Technology Center. EBL and SEM imaging was performed at the Nanotechnology User Facility at the University of Washington. This work was partially funded by the Whitaker Foundation (grant # RG-00-0356), NASA (grant # NAG9-1343), NIH (grant # RR16302), and a UW Center for Nanotechnology Fellowship (C.C.)

References and Notes

1. K. T. Brown and D. G. Flaming, Advanced micropipette techniques for cell physiology, Chichester, West Sussex, Wiley, New York **(1986)**.
2. S. M. Buttrum, E. M. Drost, W. Macnee, E. Goffin, C. M. Lockwood, R. Hatton, and G. B. Nash, Rheological response of neutrophils to different types of stimulation. *J. Appl. Physiol.* 77, 1801 **(1994)**.
3. T. W. Stone, Microiontophoresis and pressure ejection, Wiley, John and Sons, Incorporated **(1985)**.
4. J. Q. Zheng, M. Felder, J. A. Connor, and M. M. Poo, Turning of nerve growth cones induced by neurotransmitters. *Nature* 368, 140 **(1994)**.
5. A. A. Boulton, G. A. Baker, and W. Walz, Patch-clamp applications and protocols, *Neuromethods*, Humana Pr. **(1995)**.
6. B. Sakmann and E. Neher, Patch clamp techniques for studying ionic channels in excitable membranes. *Annu. Rev. Physiol.* 46, 455 **(1984)**.
7. N. Fertig, R. H. Blick, and J. C. Behrends, Whole cell patch clamp recording performed on a planar glass chip. *Biophys. J.* 82, 3056 **(2002)**.
8. N. Fertig, C. Meyer, R. H. Blick, C. Trautmann, and J. C. Behrends, Microstructured glass chip for ion-channel electrophysiology. *Phys. Rev. E State Nonlin. Soft Matter Phys.* 64, 040901 **(2001).**
9. J. Li, D. Stein, C. McMullan, D. Branton, M. J. Aziz, and J. A. Golovchenko, Ion-beam sculpting at nanometre length scales. *Nature* 412, 166 **(2001)**.
10. N. Fertig, A. Tilke, R. H. Blick, J. P. Kotthaus, J. C. Behrends, and G. ten Bruggencate, Stable integration of isolated cell membrane patches in a nanomachined aperture. *Appl. Phys. Lett.* 77, 1218 **(2000)**.
11. T. A. Desai, D. J. Hansford, and M. Ferrari, Micromachined interfaces: New approaches in cell immunoisolation and biomolecular separation. *Biomol. Eng.* 17, 23 **(2000)**.
12. T. Lehnert, M. A. M. Gijs, R. Netzer, and U. Bischoff, Realization of hollow sio2 micronozzles for electrical measurements on living cells. *Appl. Phys. Lett.* 81, 5063 **(2002)**.
13. C. Schmidt, M. Mayer, and H. Vogel, A chip-based biosensor for the functional analysis of single ion channels. *Angew. Chem.-Int. Ed.* 39, 3137 **(2000)**.
14. C. Ionescu-Zanetti, R. M. Shaw, J. Seo, Y. N. Jan, L. Y. Jan, and L. P. Lee, Mammalian electrophysiology on a microfluidic platform. *Proc. Natl. Acad. Sci. USA* **(2005)**.
15. K. G. Klemic, W. T. Baker, J. F. Klemic, M. A. Reed, and F. J. Sigworth, Patch clamping with a planar electrode array. *Biophys. J.* 80, 337A **(2001)**.
16. K. G. Klemic, J. F. Klemic, M. A. Reed, and F. J. Sigworth, Micromolded pdms planar electrode allows patch clamp electrical recordings from cells. *Biosens. Bioelectron.* 17, 597 **(2002)**.
17. J. Xu, X. B. Wang, B. Ensign, M. Li, L. Wu, A. Guia, and J. Q. Xu, Ion-channel assay technologies: Quo vadis? *Drug Discovery Today* 6, 1278 **(2001)**.
18. Y. N. Xia and G. M. Whitesides, Soft lithography. *Angew. Chem.-Int. Ed. Engl.* 37, 551 **(1998)**.
19. M. K. Chaudhury and G. M. Whitesides, Direct measurement of interfacial interactions between semispherical lenses and flat sheets

of poly(dimethylsiloxane) and their chemical derivatives. *Langmuir* 7, 1013 **(1991)**.

20. J. Fritz and M. Owen, Hydrophobic recovery of plasma-treated polydimethylsiloxane, *J. Adhesion* 54, 33 **(1995)**.

21. K. G. Klemic, J. F. Klemic, and F. J. Sigworth, An air-molding technique for fabricating pdms planar patch-clamp electrodes. *Pflugers Arch* 449, 564 **(2005)**.

22. J. Hoffman, J. Shao, C. Hsu, and A. Folch, Elastomeric molds with tunable microtopography. *Adv. Mater.* 16, 2201 **(2004)**.

23. S. Straube and A. Parekh, Inwardly rectifying potassium currents in rat basophilic leukaemia (rbl-1) cells: Regulation by spermine and implications for store-operated calcium influx. *Pflugers Archiv—Europ. J. Physiol.* 444, 389 **(2002)**.

24. L. Fierro and A. Parekh, Fast calcium-dependent inactivation of calcium release-activated calcium current (crac) in rbl-1 cells. *J. Membrane Biology* 168, 9 **(1999)**.

25. A. Tourovskaia, X. Figueroa-Masot, and A. Folch, Differentiation-on-a-chip: A microfluidic platform for long-term cell culture studies. *Lab Chip* 5, 14 **(2005)**.

26. N. Bowden, W. Huck, K. Paul, and G. Whitesides, The controlled formation of ordered, sinusoidal structures by plasma oxidation of an elastomeric polymer. *Appl. Phys. Lett.* 75, 2557 **(1999)**.

27. N. Bowden, S. Brittain, A. G. Evans, J. W. Hutchinson, and G. M. Whitesides, Spontaneous formation of ordered structures in thin films of metals supported on an elastomeric polymer. *Nature* 393, 146 **(1998)**.

Received: 3 August 2005. Revised/Accepted: 25 September 2005.